Int J Fract (2012) 176:135–149
DOI 10.1007/s10704-012-9730-2

ORIGINAL PAPER

Propagation energies inferred from deformation bands in sandstone

R. A. Schultz · R. Soliva

Received: 6 January 2012 / Accepted: 17 May 2012 / Published online: 11 July 2012

Abstract Propagation energies for five examples of deformation bands in porous sandstones from four field sites in Nevada, Utah, and France were calculated by using the J-integral approach. Pure compaction bands that accommodate primarily closing displacements from the Valley of Fire (Nevada) site have a closing-mode band propagation energy of $J_{\mathrm{I}} = 5.5 \pm 1.6\,\mathrm{kJ/m^2}$. Shear-enhanced compaction bands having subequal amounts of normal (closing) and shear strains across them from the same site have propagation energies of $J_{\mathrm{I}} = 6.11 \pm 1.8\,\mathrm{kJ/m^2}$ and $J_{\mathrm{II}} = 1.52 \pm 0.5\,\mathrm{kJ/m^2}$ for closing and shearing modes respectively. Closing- and shearing-mode band propagation energies for shear-enhanced compaction bands from the Buckskin Gulch (Utah) site, 5.63 ± 1.7 and $1.91 \pm 0.57\,\mathrm{kJ/m^2}$ and the Uchaux (France) site, 11.0 ± 3.3 and $2.35 \pm 0.7\,\mathrm{kJ/m^2}$ respectively are comparable to the values for similar structures from the Valley of Fire site. Cataclastic deformation bands at the Orange (France) site accommodate significantly larger values of shear offset than do shear-enhanced compaction bands, with a ratio of shear to closing offset that exceeds 7. The calculated closing- and shearing-mode propagation energies for these shear bands, 17.8 ± 5.4 and $3.3 \pm 1.0\,\mathrm{kJ/m^2}$ respectively are comparable to those for pure or shear-enhanced compaction bands deformed at approximately the same depth of burial. Strain softening of cataclastic compactional shear bands implies unstable shearing, whereas stable and perhaps strain-hardening shearing may be inferred for shear-enhanced compaction bands. Displacement-length scaling relations for shear-enhanced compaction bands of the form $D \propto \sqrt{L}$ are consistent with the results and with suggestions of band thickening during growth obtained from bifurcation analyses and with field observations of shear zones in porous host rock.

Keywords Deformation band · Compaction band · Weak discontinuity · Strain energy release rate · J-integral

R. A. Schultz (✉)
ConocoPhillips Company, 600 North Dairy Ashford, Houston, TX 77079-1175, USA
e-mail: richard.a.schultz@conocophillips.com

R. Soliva
Laboratoire Géosciences Montpellier, University of Montpellier II, Place E. Bataillon, 34095, Montpellier Cedex 5, France

1 Introduction

Deformation bands are tabular geologic structural discontinuities having widths of mm to cm, lengths of several meters or more, and a combination of normal and shearing offsets (displacements) across them (Aydin et al. 2006). These structures occur in porous host rocks such as sandstone and carbonate (Fossen et al. 2007) that are intriguing products of brittle strain localization having both academic and practical importance (Bésuelle 2001; Holcomb et al. 2007). In porous rocks, closing displacements across a band are accommodated

primarily by a reduction in pore volume and/or grain size due to fragmentation within the band, rather than by interpenetration of rock on either side. A subset of deformation bands, pure- and shear-enhanced compaction bands are considered to accommodate a negligible to small amount of shearing offset, respectively (e.g. Hill 1989; Mollema and Antonellini 1996; Eichhubl et al. 2010; Fossen et al. 2011) along with compaction, depending on their thickness and orientation (Soliva et al. in press), which distinguishes them from compactional or cataclastic deformation bands having larger shear offsets in relation to their thickness and length (e.g. Fossen et al. 2007; Schultz et al. 2008).

The J-integral method (Rice 1968) has occasionally been applied to investigate the propagation of fractures and deformation bands in geologic materials, including shear bands in over-consolidated clay-rich soils (Palmer and Rice 1973), crustal-scale geologic faults (e.g. Rice and Simons 1976; Rudnicki 1980; Li 1987), and compaction bands (Rudnicki and Sternlof 2005; Stanchits et al. 2009). Calculation of J for geologic structures provides a method for estimating the corresponding strain energy release rate, G, when small-scale yielding applies in the tip region. Propagation would occur when G exceeds a critical or threshold value (e.g. Rudnicki 1980; Wong 1982; Li 1987; Cox and Scholz 1988; Martel and Pollard 1989; Aydin and Schultz 1990; Kattenhorn and Pollard 1999; Olson and Cooke 2005; Baud et al. 2006; Tembe et al. 2006, 2008). J_{I} or G_{I} for closing-mode deformation have been referred to as compaction energy in the geologic literature (e.g. Rudnicki and Sternlof 2005; Rudnicki 2007; Tembe et al. 2008); we refer to both components (closing- and shearing-mode) of J more generally as band propagation energy in this paper. Values of strain energy release rate for rocks at the field scale are generally in the range of 10^2–10^5 kJ/m^2 (e.g. Atkinson and Meredith 1987; Li 1987; Martel and Pollard 1989).

Whereas the propagation of geologic cracks, faults, and shearing deformation bands is well understood in the context of fracture mechanics (e.g. Rudnicki 1980; Li 1987; Pollard and Aydin 1988; Cowie and Scholz 1992; Du and Aydin 1993; Schultz and Balasko 2003; Okubo and Schultz 2006), the controls on propagation of compaction bands remain the subject of active research. Compaction bands have been idealized as geologic anticracks that propagate at a critical value of strain energy release rate (Rudnicki and Sternlof 2005; Sternlof et al. 2005; Rudnicki 2007; Tembe et al. 2008; Schultz 2009). Chemenda (2009, 2011) modeled compaction band propagation by using a bifurcation analysis that predicted small, non-singular stress increases near band tips, seemingly consistent with the inferences of small-scale yielding and minor damage near field-scale compaction band tips made by Sternlof et al. (2005). Analyses of compaction band propagation in particular are hindered by the paucity of quantitative information on remote stress state, properties and constitutive relations of the host rock and bands, and how these may have evolved during nucleation and growth of the compaction band population. As a result of this limitation, a simplified approach is taken in this paper to investigate deformation band propagation given that a comprehensive mechanical model that incorporates all relevant aspects of band mechanics, and the observational data that could be used to verify and apply the model to specific field sites, are not yet available.

Current observations and usage clearly distinguish between two types of compaction bands. The first type, pure compaction bands (Fig. 1a), are crooked or wiggly in geometry with grain crushing and no significant component of in-plane shear offset along them (Mollema and Antonellini 1996; Eichhubl et al. 2010; Schultz et al. 2010; Fossen et al. 2011). The second type, called shear-enhanced compaction bands (Figs. 1a–c), are planar, with band thickness increasing progressively from tip to midpoint (Sternlof et al. 2005), exhibiting limited grain fracturing but significant loss of porosity by grain rearrangement, and accommodating modest shear offsets (e.g. Hill 1989) that are less than or comparable in magnitude to the band-normal closing offset (Eichhubl et al. 2010, Ballas et al. in press). Deformation bands (Fig. 1d) that are more commonly observed in a variety of rock types (e.g. Fossen et al. 2007) accommodate significantly larger magnitudes of shear displacement along them, with a magnitude of closing strain that may be comparable to that of shear-enhanced compaction bands. Deformation bands having dilational normal strain across them (Aydin et al. 2006) are not considered in this paper.

In this paper we use the J-integral method to calculate band propagation energies for five examples of pure compaction bands, shear-enhanced compaction bands, and shearing deformation bands from several sandstones from around the world. First, we revisit the value obtained for the Valley of Fire site by Rudnicki and Sternlof (2005) which continues

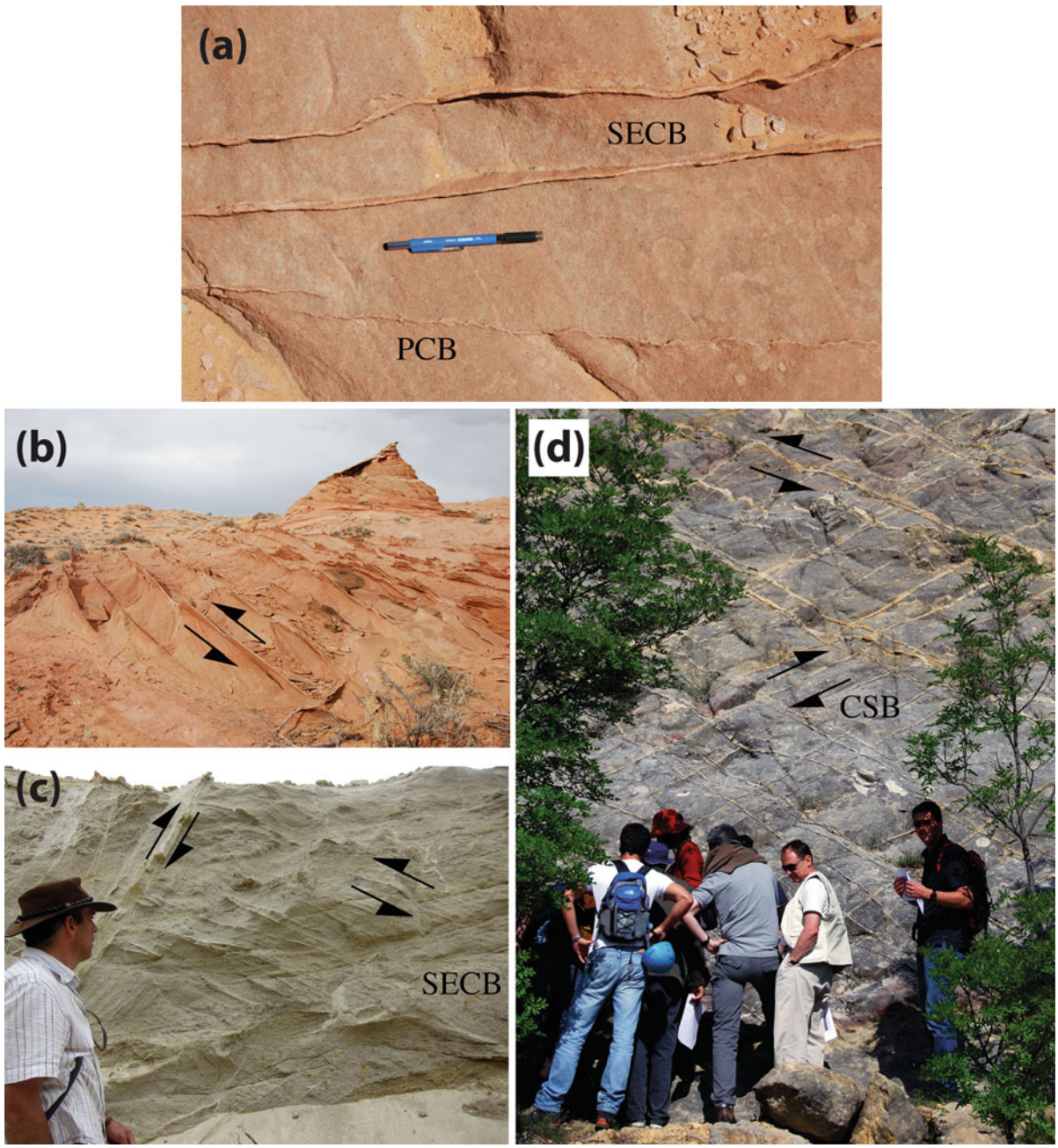

Fig. 1 Examples of deformation bands analyzed in this paper. **a** Pure (PCB) and shear-enhanced (SECB) compaction bands, Buckskin Gulch site, Utah; note stepover along PCB pair. **b** SECBs from the Buckskin Gulch site with spacing between bands ~0.5 m; sense of shear displacement given by arrows. **c** SECBs from the Boncavaï quarry, Uchaux, France, site. **d** Cataclastic compactional shear bands from the Orange quarry, France, site

to provide a baseline for studies of compaction (or propagation) energy in sandstones, both from the field and in the laboratory (e.g. Holcomb et al. 2007; Tembe et al. 2008; Stanchits et al. 2009). Next, we calculate the closing- and shearing-mode propagation energies for bands from this and other field sites and discuss the implications for porous rock deformation.

2 Field localities

Deformation bands from four field sites are analyzed in this paper. The first site is located in Valley of Fire State Park, southern Nevada, USA. Geologic and structural relations are summarized by Eichhubl et al. (2004), Flodin and Aydin (2004), and Sternlof et al. (2005). The Aztec Sandstone that hosts the compaction bands has a porosity of 22.7 % which is reduced to 14.3 % in shear-enhanced compaction bands and 12.2 % in pure compaction bands (Eichhubl et al. 2010). According to Eichhubl et al. (2010), the site was buried to a depth of ~600 m at the time of deformation, a value that is subject to some uncertainty related to the timing and geometry of the overlying thrusted geologic section. Strike-slip and closing offsets inferred along the bands (Eichhubl et al. 2010) were related to a contractional tectonic regime (Hill 1989; Flodin and Aydin 2004).

The original work on compaction bands from the Valley of Fire site concluded that thick compaction bands in one part of this site had accommodated both closing and shear strains, whereas crooked bands accommodated primarily closing normal strain (Hill 1989). Subsequent work did not consider shearing displacements along thick compaction bands at the site, so that only the closing-mode component of G was calculated for these bands (Rudnicki and Sternlof 2005; Rudnicki 2007). More recently, shearing offsets having magnitudes perhaps comparable to the closing offsets were recognized or inferred along the thick compaction bands (Eichhubl et al. 2010). Both closing- and shearing-mode components to the band propagation energy for thick shear-enhanced compaction bands at this site are calculated in this paper.

The Buckskin Gulch site in southwestern Utah, USA, is described by Mollema and Antonellini (1996), Schultz (2009), Schultz (2011), Solum et al. (2010), and Fossen et al. (2011). Both pure and shear-enhanced compaction bands are known from this site (Fig. 1a, b), with reverse (contractional) offsets of a few mm locally observed along the latter. Pure compaction bands from this site are not considered further in this paper. The host Navajo Sandstone has a porosity of 20–25 % which is reduced within the shear-enhanced compaction bands to "a few percent" (Mollema and Antonellini 1996). In this paper we choose values of 22 % for the host rock porosity and 20 % for the band porosity, consistent with measured values of shear-enhanced compaction bands from the other sites. The thickness of overburden at the time of deformation is uncertain, with estimates between 1 and 1.5 km (Schultz 2009; Fossen et al. 2011).

A third site hosting shear-enhanced compaction bands was reported by Soliva et al. (2011, in press) and Ballas et al. (in press). The Uchaux site is located in the *Bassin du Sud-Est*, south-central France in the Boncavaï quarry northeast of Mornas, France (see Saillet 2009 and Saillet and Wibberley 2010 for description). The host sandstone is coarse-grained, poorly cemented and hence friable, with a porosity of 28 % and band porosity of 23 %, and a depth of burial of approximately 400 m (Saillet 2009; Ballas et al. in press). Conjugate sets of shear-enhanced compaction bands are observed (Fig. 1c) with reverse offsets related to a contractional tectonic regime at the time of deformation (Soliva et al. in press).

We also investigate deformation bands from the Quartier de l'Etang quarry in Orange, southern France (Wibberley et al. 2007; Saillet and Wibberley 2010; Klimczak et al. 2011; Chemenda et al. 2012). These bands are cataclastic deformation bands (Fossen et al. 2007) that exhibit closing as well as shear offsets (Fig. 1d). The finer-grained nature of the host sandstone and the abundance of band intersections and pre-existing marker beds permit the ready observation and measurement of shear offsets along the bands. These bands are referred to as compactional shear bands in this paper. The host rock has a porosity of 29 %, reduced to 21 % along the bands (Saillet 2009). Similar to the Buckskin Gulch and Uchaux sites, the deformation bands at the Orange site exhibit reverse offsets consistent with a contractional tectonic regime at the time of deformation, with an inferred depth of burial of about 600 m.

3 Analysis

We follow the approach of Rudnicki and Sternlof (2005) in their analysis of compaction bands in sandstone, noting that J can also be obtained by other formulations that involve parameters such as host-rock modulus (Palmer and Rice 1973; Rudnicki 1980) and strength changes related to slip weakening (Kanninen and Popelar 1985; Li 1987) that may not generally be available from field-based studies of deformation bands. Sternlof et al. (2005) interpreted compaction bands as closing-mode anticrack-like structures and, like Rudnicki (2007) and Tembe et al. (2008), inferred conditions of small-scale yielding at the band tips. Chemenda (2011) interpreted compaction bands

instead as non-brittle structures growing under nearly general plastic yielding of the host rock with minor stress amplification near band tips. The formulation of Rudnicki and Sternlof (2005) is not dependent on the degree of stress concentration at compaction band tips, so it is applicable to either interpretation (see also Lawn 1993, pp. 66–70).

Band propagation energies represent the work done by remote tectonic loading to propagate a deformation band a unit distance into the host rock; the analysis does not consider thermal or radiated energy that may also be released depending in part on strain rate (Togo and Simamoto 2012) but that lack direct field evidence from the outcrop sites. The strain energy release rate calculated in this paper for a deformation band has been associated with a closing mode of rock deformation in which volume loss is related to Hertzian cracking at grain-to-grain contacts, frictional sliding between grains, and pore collapse (e.g. Rudnicki 2007; Holcomb et al. 2007). Values of G or J calculated for deformation bands in this paper or in the literature are considered to be equal to or greater than a critical value G_c or J_c required for band propagation (e.g. Rudnicki and Sternlof 2005).

3.1 Calculation of band propagation energy

Rudnicki and Sternlof (2005) used a J-integral approach to calculate the closing-mode propagation energy for shear-enhanced compaction bands from the Valley of Fire site. In their plane-strain analysis, displacements applied far from the band (at a perpendicular distance $h/2$; Fig. 2) produced normal (closing) strains in the host rock and within the compaction band, which is taken to be semi-infinite in length and much larger than h. After some manipulation and simplification that assume reasonable rock properties in a porous sandstone, such as a contrast in modulus between host rock and band of less than about a factor of two (consistent with later experimental work by Kaproth et al. 2010), they obtained the simple expression

$$G_{\mathrm{Ic}} = \sigma_n \varepsilon_p \varsigma h \tag{1}$$

in which σ_n is the driving stress, corresponding approximately to the compressive normal stress resolved on the band, obtained from considerations of the local tectonic stress state at the time of deformation (Sternlof et al. 2005; Schultz 2009; Eichhubl et al. 2010); ε_p is the closing (normal) strain due to compaction across the band; and ζ is the ratio of band spacing to thickness, so that ζh is the maximum band thickness. This expression is comparable to that later obtained by Tembe et al. (2008). Compressive normal stress and closing normal strain are taken to be positive in this analysis. Using Eq. (1) along with σ_n = 10–60 MPa, $\varepsilon_p = 0.1$, and $\zeta h =$ 1 cm (i.e. bands $\zeta h = 1$ cm thick spaced $h = 1$ m apart) Rudnicki and Sternlof (2005) obtained a closing-mode band propagation energy in the range of 10–60 kJ/m^2.

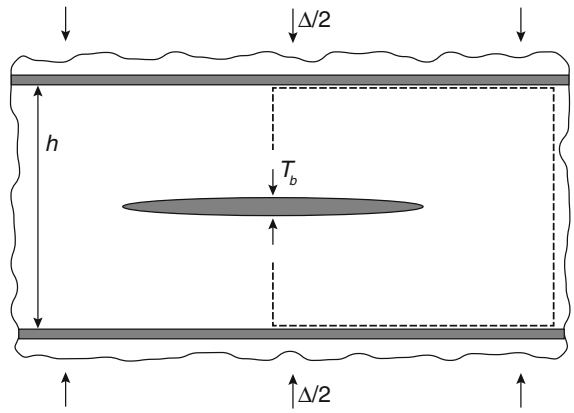

Fig. 2 Model setup following Rudnicki and Sternlof (2005); see text for parameters and discussion

Following Sternlof et al. (2005), the band-normal displacement associated with pore collapse within shear-enhanced compaction bands can be related to the change in porosity between host sandstone and the band. Neglecting grain cracking or dissolution and elastic compaction or volume change of the grains, the normal (closing) displacement associated with the reduction in pore volume is given by

$$D_c = \frac{T_b\,(\phi_i - \phi_b)}{(1 - \phi_i)} \tag{2}$$

in which T_b is the band thickness, ϕ_i is the initial porosity of the host rock, and ϕ_b is the reduced porosity of the band (Soliva et al. in press). The plastic normal strain associated with porosity reduction is then given by

$$\varepsilon_p = \frac{D_c}{T_b} = \frac{(\phi_i - \phi_b)}{(1 - \phi_i)} \tag{3}$$

(see also Sylte et al. 1999) which increases with the difference in porosity between the host rock and the band. Although the closing strain associated with compaction and porosity reduction within a band is probably a three-dimensional quantity (Schultz 2011), the uniaxial normal strain is used in this paper for convenience given

the current absence of measurements of the band-parallel components of closing strain. The value of closing displacement depends on the band thickness, here taken as the average value of the thickness measurements of bands from a particular study locality. Equation (1) can be rewritten as

$$G_{Ic} = \sigma_n \varepsilon_p T_b = \sigma_n D_n \tag{4}$$

in which D_n is the closing displacement across the band.

Because strain energy release rates (e.g. Kanninen and Popelar 1985, p. 163) or J-integrals (Hasanpour and Choupani 2008) for the three displacement modes can be additive, the normal (closing) and shear components of displacement could be summed to obtain the total resultant displacement across the band (see also Crouch and Starfield 1983, pp. 208–210) assuming that the displacements (offsets) are reasonably small. However, the closing and in-plane shearing displacements are considered separately in this paper given that the rates of accumulation of closing and shearing displacements, the possible interactions between compaction and shearing within a band, and the onset of deformation mechanisms such as cataclasis, are not well constrained.

Normal and shear driving stresses acting to promote normal and shear offsets along deformation bands are considered as follows. Previous work assumed that the normal stress associated with closing-mode deformation along compaction bands was approximately equal to the resolved far-field normal stress on the bands (Rudnicki and Sternlof 2005; Rudnicki 2007; Tembe et al. 2006, 2008), which assumes that the resistance of host-rock grains to compaction is much smaller than the resolved compression. This approach is adopted in this paper, so that the normal component of driving stress σ_{nd} is taken to be approximately equal to the normal stress resolved on the band σ_n. Although deformation bands can be defined more generally in relation to the plastic strain increment tensor rather than to the stress tensor (especially for non-associated plastic flow; Borja and Aydin 2004), the stress-based approach is sufficient for the present analysis.

Laboratory work demonstrates an increase in axial load during growth of shear-enhanced compaction bands (Stanchits et al. 2009), implying stable growth and, perhaps, a strain-hardening band rheology. In this case band growth is taken to initiate at a value of shear driving stress σ_{sd} (Palmer and Rice 1973; Li 1987) corresponding to the resolved (peak) shear stress σ_s on the bands. In contrast, compactional shear bands nucleate at or near the peak resolved shear stress with growth and accumulation of shear offsets occurring post-peak, indicating a strain-softening rheology (Mair et al. 2000; Kaproth et al. 2010) similar to shear bands in soil (Palmer and Rice 1973) and geologic faults in rock (Rudnicki 1980; Li 1987). We take $\sigma_{sd} = (\sigma_s - \sigma_r)$, where σ_r is the residual shear resistance of the compactional shear band, with $\sigma_{sd} / \sigma_s \sim 0.1$ following laboratory work reported by Kaproth et al. (2010). Band propagation energies for closing and shearing modes are then given approximately by

$$\begin{aligned} J_{\mathrm{I}} &= \sigma_{nd} D_n \\ J_{\mathrm{II}} &= \frac{\sigma_{sd} D_s}{2} \end{aligned} \tag{5}$$

in which J_{I} is the closing-mode energy, J_{II} is the in-plane shearing-mode energy, σ_{nd} and σ_{sd} are the normal and in-plane-shear driving stresses respectively, D_n is the closing displacement, and D_s is the in-plane shear displacement across the band (since the plastic shear strain $\gamma_p = D_s / 2T_b$). The expression for shearing-mode energy is comparable to that of Torabi and Alikarami (2012) while explicitly incorporating shear driving stress and total shear displacement across a band.

J-integral methods were used previously by Yoda (1980) to evaluate mixed-mode propagation paths. Values of $J_{Ic} = 175\,\mathrm{kJ/m^2}$ and $J_{IIc} = 173\,\mathrm{kJ/m^2}$ were obtained for JIS S25C steel from torsional tests of a thin-walled tube, with fracture growth occurring in the direction of maximum strain energy release rate. More recently, Sutton et al. (2000) used a CTOD criterion to infer that mixed-mode fracture growth occurs in the direction where the yield criterion was first met. Given in-plane propagation of shear-enhanced compaction bands and compactional shear bands as inferred from field relations, we infer that the bands propagated under pre-peak yielding conditions, as has been suggested for growth of shear structures in porous rocks (e.g. Du and Aydin 1993; Schultz and Balasko 2003; Okubo and Schultz 2006).

For mode-I cracks having traction-free surfaces, J is both path independent (i.e. has the same value regardless of the contour or path taken around the crack tip) and independent on the position along the crack (e.g. Kanninen and Popelar 1985). However, for geologic structures such as faults and deformation bands that support normal and/or shear tractions along them (e.g. Pollard and Segall 1987), J is path independent but

its value depends on the starting and ending positions along the band (Rudnicki 1980; Li 1987). We choose the midpoint along a band (dashed contour in Fig. 2), corresponding to the average band thickness, as the reference point for the closing and shearing displacements to assure consistency for bands having variable lengths.

3.2 Determination of key parameters

3.2.1 Normal and shear stress on the bands

Normal and shear stresses resolved onto the bands were calculated from the tectonic regime at each site. For the Valley of Fire site, the two sets of shear-enhanced compaction bands have trends of N15°W (for the inferred right-lateral set) and N61°E (for the inferred left-lateral set), as reported by Eichhubl et al. (2010). The bisector of the 76° angle between the band sets orients the bands with a band-normal vector of $\theta = 90° - 76°/2 = 52°$ to the maximum horizontal compressive principal stress σ_1; the other horizontal principal stress in the strike-slip regime is σ_3. The intermediate principal stress $\sigma_2 = \sigma_v$, equal to $\rho\, gz$, where ρ is the effective density of overburden (taken to be dry rock density minus that of water), g is gravitational acceleration, and z is the depth below the present ground surface of the site at the time of deformation. Following Jaeger et al. (2007), the normal and shear stresses σ_n and τ are calculated by using the values of σ_1 and σ_3 with $\sigma_1 = q\,\sigma_3$ and $\theta = 52°$ (Table 1) where $q = \left[\sqrt{(\mu^2+1)} + \mu\right]^2$, in which μ is the static friction coefficient of the host rock and assuming plane-strain conditions so that $\sigma_v = \sigma_2 = \nu(\sigma_1 + \sigma_3)$. The far-field principal stresses are, after algebraic manipulation, then given by $\sigma_1 = \sigma_v/[\nu(1+1/q])$, where ν is Poisson's ratio (taken to be 0.2).

For the remaining three sites, the contractional (thrust faulting) tectonic regime requires that $\sigma_1 = q\,\sigma_3 = q\,\sigma_v$, where σ_v is again $\rho\, gz$. σ_v was calculated by using hydrostatic pore-water pressure and approximate dry densities of 2,250 kg/m^3, with paleodepths z of 600 m for Valley of Fire, 1 km for Buckskin Gulch, and approximately 600 m for Orange (Saillet 2009) and ~400 m for Uchaux. Because paleodepths at each site are not precisely determined given large uncertainties in the estimates of burial from stratigraphic reconstructions, uncertainties of ±30 % in paleodepths, and hence paleostress state and stress magnitudes, are chosen in this paper. Paleodepths are taken to be 600 ± 180 m for Valley of Fire, 500 ± 150 for Uchaux and Orange, and 1,000 ± 300 m for Buckskin Gulch.

Given σ_v, the two horizontal remote principal stresses are calculated by using a friction coefficient for the host rock of $\mu = 0.5$ (Karner et al. 2005) for the Valley of Fire, Buckskin Gulch, and Uchaux sites, and $\mu = 0.6$ for the finer-grained sandstone at the Orange site. These values correspond to $q = 2.62$ and 3.12, respectively. Because the principal stress magnitudes are limited by the frictional resistance of the rock, they provide upper limits on the peak stress magnitudes for deformation banding, given that bands form at or before peak-stress levels are reached (e.g. Olsson 1999, 2000; Gutierrez 2011). Differences in the values for μ and q contribute smaller uncertainties to J than those in depth. For example, for the Valley of Fire site, a 43 % reduction in q, from 2.62 to 1.51 (corresponding to a minimum value for typical rocks of $\mu = 0.2$), corresponds to reductions in normal stress of 11.6 %, shear stress 23.7 %, J_I 12 %, and J_{II} 24.3 %,

Table 1 Remote and resolved stresses inferred for deformation bands

Location	σ_1 (MPa)[a]	σ_3 (MPa)	Band-normal angle θ, (°)	σ_n (MPa)	τ (MPa)
Valley of Fire, NV[b,c]	26.59	10.16	0°	26.59	0.00
Valley of Fire, NV[b,d]	26.59	10.16	52°	14.64	9.34
Buckskin Gulch, UT	32.07	12.25	54°	19.10	9.43
Uchaux, France	16.04	6.125	47°	10.74	4.94
Orange, France	16.04	6.125	52°	9.88	4.81

[a] σ_1 calculated by using $\mu = 0.5$ (first three sites) and 0.6 (Orange site)
[b] $\sigma_v = \sigma_2 = 7.35$ MPa
[c] Pure compaction bands
[d] Shear-enhanced compaction bands

assuming no changes in band thickness or plastic strain. The uncertainties in stress magnitude, associated with paleodepth, thus contain that from friction coefficient and principal stress ratio.

3.2.2 Plastic normal strain and normal displacement

Previous work has shown that normal (closing) displacements appear to be relatively constant along pure (Fossen et al. 2011) and shear-enhanced compaction bands (Sternlof et al. 2005), whereas shear displacements along both shear-enhanced compaction bands and compactional shear bands vary systematically with band thickness and length (Schultz et al. 2008; Schultz 2009). Values for closing and shearing displacements used in this paper, listed in Table 2, are average values measured across bands from each study area. Closing displacements $D_c = D_n$ were calculated from (2) by using the average band thickness reported from each field site. For the Valley of Fire shear-enhanced compaction bands, the band-normal vector to σ_1 was 52° based on the difference in trend of the inferred conjugate left-lateral and right-lateral bands (Eichhubl et al. 2010). For the Buckskin Gulch, Uchaux, and Orange shear-enhanced compaction bands, band-normal angles based on the conjugate band geometries of 54°, 47°, and 52° respectively, were used. This approach is consistent with the Valley of Fire and Buckskin Gulch shear-enhanced compaction bands forming contemporaneously with pure (wiggly or crooked) compaction bands there having band-normal angles of $\sim$ 0° to the horizontal, and therefore taken to be oriented normal to the maximum (horizontal) compressive stress at the time of their formation (e.g. Hill 1989; Eichhubl et al. 2010; Fossen et al. 2011) assuming coaxial deformation.

Values of porosity change for pure compaction bands have been reported from the Valley of Fire site. Eichhubl et al. (2010) notes a reduction in porosity from 22.7 to 12.2 % (or expressed as intergranular volume, from 27.3 to 19.8 %), corresponding to a smaller degree of porosity reduction than that measured for the shear-enhanced compaction bands (expressed as intergranular volume) from the site. Band widths are about 2–3 times the maximum grain size of the host rock, corresponding to approximately 2 mm. J_I is calculated for these pure compaction bands by using (5) with their closing displacements calculated by using Eq. (2), a thickness of 2 mm, and $\sigma_{nd} = \sigma_1 = 26.6$ MPa (value for Valley of Fire, Table 2).

3.2.3 Shear displacement

Shearing displacements along deformation bands can be challenging to measure in the field. Values can be obtained at the intersections between bands and pre-existing passive markers, such as eolian cross-beds or stratification. Shearing along shear-enhanced compaction bands in the Valley of Fire site is inferred to be of strike-slip sense (Hill 1989; Eichhubl et al. 2010 and personal communication 2011), or subparallel to the bedding, making values of shear displacement uncertain given the scarcity of pre-existing markers oriented at high angles to the bands. Certain band geometries that are reminiscent of stepovers along strike-slip structures having various degrees of linkage (Du and Aydin 1993; Schultz and Balasko 2003; Okubo and Schultz 2006), tentatively observed at the site (RA Schultz unpublished data 2012), may support

Table 2 Parameters for deformation bands

Location	ϕ_i	ϕ_b	ε_p	T_b (mm)	D_c (mm)	D_s (mm)[b]	D_s/D_c
Valley of Fire, NV[a,c]	0.273	0.198	0.103	2.0	0.206	−0−	0.0
Valley of Fire, NV[a,d]	0.273	0.225	0.066	6.32	0.417	0.326	0.78
Buckskin Gulch, UT[d]	0.22	0.2	0.0256	11.5	0.295	0.405	0.58
Uchaux, France[d]	0.28	0.23	0.0694	14.7	1.02	0.952	0.933
Orange, France[e]	0.29	0.21	0.111	16.2	1.80	13.6	7.55

[a] Porosities listed for Valley of Fire site are intergranular volume (IGV) that include quartz cementation
[b] D_{sc} calculated from D_c and band angle to σ_1 for SECBs
[c] Pure compaction bands
[d] Shear-enhanced compaction bands
[e] Compactional shear bands; D_s is the measured average shear offset arross the bands

interpretations of shear-enhanced compaction bands there having small strike-slip offsets. Eichhubl et al. (2010)
suggested that the magnitude of shear displacement along the bands was approximately one-tenth the band thickness, or on the order of 1 mm. Shear-enhanced compaction bands at the Buckskin Gulch site display a reverse (contractional) sense of displacement (Mollema and Antonellini 1996; Schultz et al. 2010); values observed at various places at the site are on the order of 1–2 mm. Shear displacements along shear-enhanced compaction bands at the Uchaux site are difficult to observe and measure due to the coarse-grained nature of the host sandstone (average grain size ~0.65 mm); a maximum value of ~1 mm has been inferred from magnified petrographic thin sections of the bands (Soliva et al. in press).

Normal strain across a deformation band can produce an apparent shear displacement of a pre-existing passive marker. For a deformation band of given thickness that intersects a marker at an angle α, the apparent shear displacement due to compaction, D_{sc}, is related to the normal displacement due to compaction, D_c, by $D_{sc} = D_c/\tan\alpha$ (Soliva et al. in press). Rather than relying on ambiguous or imprecise field estimates of shear displacement magnitude for the shear-enhanced compaction bands investigated in this paper, we choose to calculate D_{sc} by using the angle between the band and the direction of maximum compressive principal stress σ_1. Angles used are 38° (Valley of Fire site), 37° (Buckskin Gulch site), 43° (Uchaux site), and 38° (Orange site); pure compaction bands at the Valley of Fire set have an angle of 90°. The calculated values of apparent shear displacement are geometrically compatible with compaction across a band of given thickness that is inclined to the direction of compaction (assumed to be parallel to σ_1) and, interestingly, are consistent with the qualitative observations or inferences of shear offset magnitude and band thickness obtained for shear-enhanced compaction bands from the three field sites.

In contrast, shear offsets along the cataclastic deformation bands in Orange quarry are well resolved in the field, averaging 13.6 mm, or 7.5 times the average closing normal displacement calculated by using Eq. (2), 1.8 mm (Table 2). This large magnitude of shearing offset is consistent with that noted by Eichhubl et al. (2010) for cataclastic deformation bands at the Valley of Fire site and exceeds that calculated trigonomically from the band orientation and thickness in this paper, reinforcing the interpretation that shear-enhanced compaction bands only accommodate closing and shear strains compatible with the porosity reductions, band orientations, and band thicknesses, without further weakening or strain localization in shear.

Values of band propagation energy are subject to uncertainty from several sources. The onset of localized compactional deformation in porous granular solids remains challenging to pin-point in experiments or in the field (e.g. Smith et al. 1992; Karner et al. 2003), leading to some uncertainty in the values for driving stress used in (5). Similarly, compaction and plastic normal strain in deformation bands were represented in (3) by a mechanical reduction in porosity. Detailed work shows, however, that pore volume may also be reduced in these bands by chemical diagenetic processes including precipitation and cementation of silica around the grains (Milliken et al. 2005). Although the degree of cementation in the bands studied appears to be less apparent than the porosity loss due to grain rearrangement, the plastic normal strains calculated from (3) and used in (5) provide an upper limit to the degree of compaction across the bands. These uncertainties appear to be comparable to or less than the uncertainty in burial depth, taken to be ±30 % in this paper.

4 Results and implications

Previous values of critical strain energy release rate from the Valley of Fire site, calculated by using normal (closing) strains across the shear-enhanced compaction bands, were $G_{Ic} = 10{-}60\,\mathrm{kJ/m^2}$ (Rudnicki and Sternlof 2005). These values did not incorporate pore-water conditions typical of subsurface conditions within the Earth and inferred for the Valley of Fire site (Tembe et al. 2008; Schultz 2009; Eichhubl et al. 2010) at the time of deformation. Taking hydrostatic pore pressure into account by using adjusted rock densities and a Biot coefficient of 1.0 ($\rho = \rho_{rock} - \rho_{water} = 2{,}250 - 1{,}000 = 1{,}250\,\mathrm{kg/m^3}$) results in reduced values for the resolved normal stress on the bands of 7–30 MPa, and corresponding values of $G_{Ic} = 7{-}30\,\mathrm{kJ/m^2}$, which are used as the reference values in this paper.

The closing-mode band propagation energy obtained in this paper for shear-enhanced compaction bands from the Valley of Fire site is $J_I = 6.11 \pm 1.8\,\mathrm{kJ/m^2}$ (Table 3). If it is assumed that the bands' near-tip

Table 3 Band propagation energies

Location	Type of band	J_I (kJ/m^2)	J_{II} (kJ/m^2)
Valley of Fire, NV	PCB	5.5 $\pm$ 1.6	0
Valley of Fire, NV	SECB	6.11 $\pm$ 1.8	1.52 $\pm$ 0.46
Buckskin Gulch, UT	SECB	5.63 $\pm$ 1.7	1.91 $\pm$ 0.57
Uchaux, France	SECB	11.0 $\pm$ 3.3	2.35 $\pm$ 0.71
Orange, France	CSB	17.8 $\pm$ 5.4	3.27 $\pm$ 0.98

PCB pure compaction band, *SECB* shear-enhanced compaction band, *CSB* compactional shear band

regions may be characterized by small-scale yielding, so that $J = G$, then the value of band propagation energy obtained for these bands in this paper is consistent with the previous work while refining the magnitude of the propagation energy to the lower part of the updated previous range ($J_I = G_{Ic} =$ 7–30 kJ/m^2).

An estimate of J_I for pure compaction bands from the Valley of Fire site was also made, with $J_I = 5.5 \pm 1.6$ kJ/m^2 (Table 3). This value is comparable to the closing-mode value for the shear-enhanced compaction bands from the same host sandstone at that site ($J_I = 6.11 \pm 1.8$ kJ/m^2. The comparable values of J_I for both types of compaction bands indicate that grain crushing and the associated increase in plastic normal strain was approximately compensated by the smaller widths of pure compaction bands, implying a comparable tendency to propagate through the host sandstone. This finding may be relevant to theoretical investigations of compaction localization that are based on grain fragmentation (Das et al. 2011) which utilize the material properties such as grain size and shape, stress state, and deformation mechanism within the compaction bands (i.e. fragmentation or pore collapse).

Values of J_I and J_{II} calculated in this paper for deformation bands from all field sites are listed in Table 3. Closing-mode band propagation energies range from approximately 5–18 kJ/m^2 and appear to be relatively independent of paleodepth (Fig. 3a) and plastic normal strain (not shown), demonstrating the interrelationship between stress state and rock properties such as porosity change in deformation band formation. Shearing-mode band propagation energies J_{II} are approximately 1–3 kJ/m^2 and depend on the ratio of shearing to closing displacements (Fig. 3b). Shear-enhanced compaction bands are characterized by subequal values of D_s/D_c between about 0.7 and 1.0, placing their values of band propagation energy (J_{II}) intermediate between those

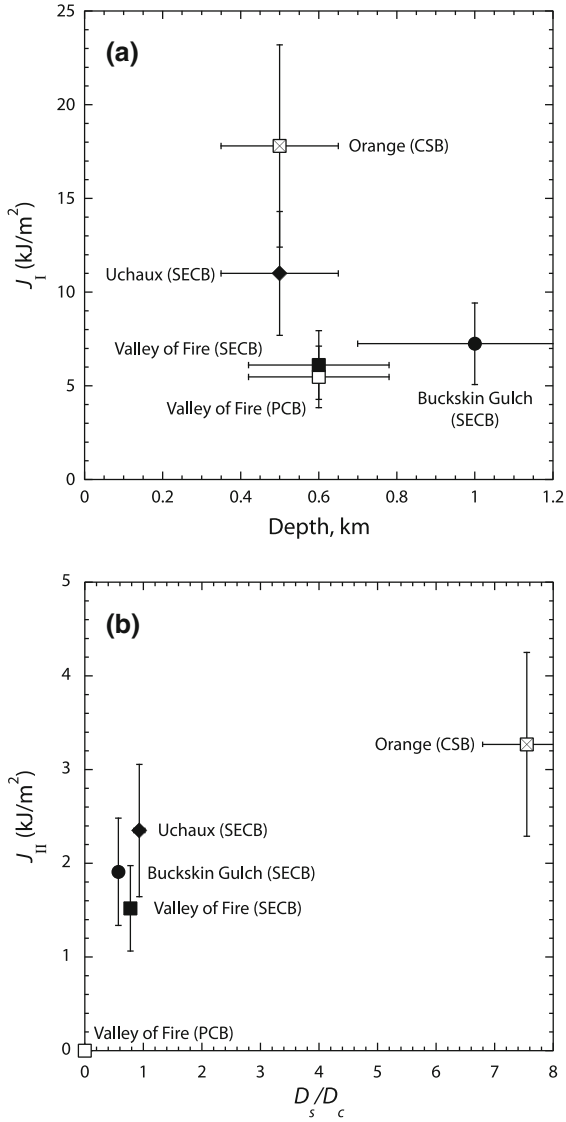

Fig. 3 Closing **a** and shearing **b** components of band propagation energy, J_I and J_{II}, respectively, from each field site. Uncertainties shown are ± 30 % in J and depth, and ± 10 % in D_s/D_c

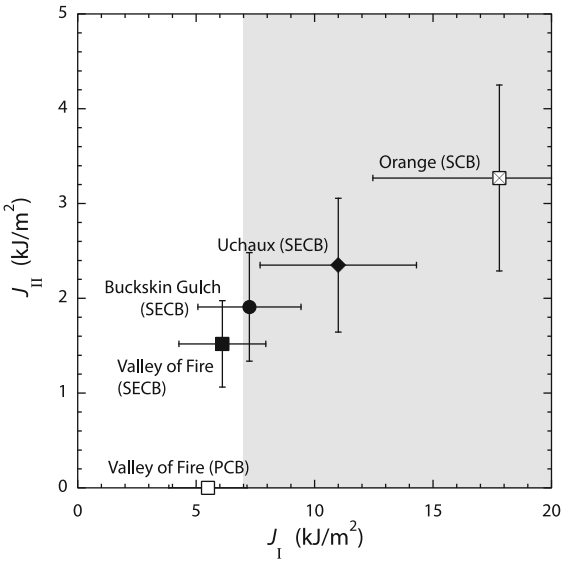

Fig. 4 Closing-mode and shearing-mode band propagation energies from each field site plotted against each other; uncertainties as in Fig. 3. *Shaded range* for J_I in **a** calculated for Valley of Fire shear-enhanced compaction bands assuming hydrostatic pore-water conditions ($J_I = G_{Ic} = 7$–$30\,\mathrm{kJ/m^2}$)

of pure compaction bands (for which $J_{II} = 0$) and compactional shear bands. The values of D_{sc} are limited trigonometrically by band thickness and angle of the band to the direction of maximum closing strain (i.e. to the σ_1 direction for coaxial deformation). Comparable values of normal and shear offsets, and hence closing and shear components of the band propagation energy, are found for shear-enhanced compaction bands from all three field sites. As a result, a wider range of values is calculated for J_I than for J_{II} (Fig. 4).

The closing-mode band propagation energy for shear-enhanced compaction bands from the Uchaux site, $J_I = 13.3 \pm 4.0\,\mathrm{kJ/m^2}$, is comparable to that for similar structures from the Valley of Fire site (Table 3). It appears that loose, poorly consolidated sands and sandstones deformed at relatively shallow depths (i.e. 400–600 m) at either site may generate shear-enhanced compaction bands with modest values of J_I.

The values of J_I obtained in this paper are generally smaller than those determined in laboratory studies on small rock samples (assuming that $J_I = G_I$). For example, Vajdova and Wong (2003) obtained a lower bound to G_I for Bentheim Sandstone of $16\,\mathrm{kJ/m^2}$, whereas Tembe et al. (2006) estimated values of G_I for Berea and Bentheim Sandstones of 6–$43\,\mathrm{kJ/m^2}$. Stanchits et al. (2009) obtained values using the Rudnicki and Sternlof (2005) method (Eq. 1 in this paper) for notched samples of water-saturated Bentheim Sandstone of $G_I = 23$–$53\,\mathrm{kJ/m^2}$. The values reported by Stanchits et al. (2009) assumed comparable values for ε_p (0.1 in their paper, with values of host-rock and band porosity of 22–24 % and 10–16 % respectively) and band thicknesses of $\zeta h = T_b = 0.8 - 0.9\,\mathrm{mm}$, but with normal (axial) stresses in excess of 200 MPa. The normal stress applied to the laboratory samples was thus 8–20 times greater than that inferred for the field sites (Table 1). The narrow zones of intense grain crushing and angular band geometries noted by Fortin et al. (2006) and Stanchits et al. (2009) appear similar to those of pure compaction bands from field sites such as Valley of Fire. Interestingly, the large values of axial stress in the experiments could potentially be offset in (1) or (5) by corresponding increases in band thickness, assuming the same values of plastic normal strain, to achieve approximate parity between the field-based (Table 3) and laboratory values (Stanchits et al. 2009) of G_I. Chemenda's (2011) analysis of compaction band growth suggests more generally that a combination of large differential stress magnitude, small sample size, and evolving constitutive parameters during deformation of the host rock contribute to the discrepancies between field and laboratory values.

The values of J_I and J_{II} for Buckskin Gulch assumed a band porosity of 20 %, consistent with shear-enhanced compaction bands from the other sites but somewhat larger than what might be interpreted from the qualitative description given by Mollema and Antonellini (1996). A much smaller value of band porosity would produce a larger value of plastic normal strain (e.g. a band porosity of 2 % with host rock porosity of 22 % would imply ε_p of 0.256) and a correspondingly larger value for J_I (equal to $72.3 \pm 21.7\,\mathrm{kJ/m^2}$ in this example). Precise measurements of band porosity for Buckskin Gulch shear-enhanced compaction bands are needed to more definitively compare the band propagation energies to those from other sites.

Compactional shear bands at the Orange site accommodate much larger values of shear offset than do shear-enhanced compaction bands, with ratios of shear to closing offset of $D_s/D_c > 7$ (Fig. 3b, c). J_{II} for these bands, $3.3 \pm 1\,\mathrm{kJ/m^2}$, is comparable to that for shear-enhanced compaction bands deformed at approximately the same depth of burial (i.e. the Valley of Fire and Uchaux sites; Table 3). Cataclasis in the

compactional shear bands involves grain comminution and shearing at grain-to-grain contacts within a band (e.g. Fossen et al. 2007; Eichhubl et al. 2010). Davies et al. (2012) demonstrate that the strain energy released by grain fragmentation can facilitate strain localization by reducing the effective frictional resistance of grain contacts and force chains, perhaps accounting for larger shearing displacements occurring at smaller values of shear driving stress than would be expected for shear-enhanced compaction bands. A similar explanation could be offered as an interpretation of the results for pure compaction bands, where grain fragmentation might facilitate band localization and propagation.

Shear strain γ_s along the shear-enhanced compaction bands from all sites, calculated from D_s and average band thickness, is between 0.01 and 0.03, whereas that of compactional shear bands in Orange is 0.42, corresponding to an increase of an order of magnitude despite similarities in band thickness and closing normal strain among the bands. Because the rate-and-state frictional stability of quartz-rich and phyllosilicate-poor aggregates tends to decrease from velocity-strengthening to velocity-weakening behavior with increasing shear strain (Ikari et al. 2011), the compactional shear bands in Orange, and perhaps those in similar rocks elsewhere, might be expected to exhibit evidence for unstable slip within the bands, such as planar slip surfaces, whereas shear-enhanced compaction bands may remain velocity-strengthening during their evolution. This inference is consistent with laboratory work on deformation bands that demonstrates a switch in deformation mechanism, from stable, strain-hardening flow to more localized strain-softening behavior with increasing amounts of remote strain (Hirth and Tullis 1989; Mair et al. 2000; Fossen et al. 2007).

The results have implications for the displacement-length scaling of pure and shear-enhanced compaction bands. The thicknesses of pure (wiggly or crooked) compaction bands appear to be relatively constant over their variable lengths (e.g. Fossen et al. 2011), so that displacement-length scaling, in which band thicknesses or closing displacements would increase as a function of band length (e.g. Schultz et al. 2008), does not appear to apply. On the other hand, the thicknesses and shear offsets of shear-enhanced compaction bands do scale with band length (Rudnicki 2007; Schultz et al. 2008; Tembe et al. 2008; Schultz 2009) such that $T_b = \beta L^{1/2}$. Measurements of shear-enhanced compaction bands from the two sites for which band lengths are available indicate (Schultz 2009) that $\beta = 0.0019\,\mathrm{m}^{1/2}$ (Valley of Fire site) and $\beta = 0.0063\,\mathrm{m}^{1/2}$ (Buckskin Gulch site). Because the normal and shear displacements are related trigonometrically by band orientation ($D_s = D_{sc} = D_c/\tan\alpha$), the plastic shear strain can be related to the plastic normal strain by $\gamma_s = \varepsilon_p/2\tan\alpha$. Combining the latter expression with $T_b = \beta L^{1/2}$ then gives

$$D_s = \beta\varepsilon_p\sqrt{L}\,\cot\alpha \tag{6}$$

For angles of $\alpha = 38°$–$52°$ noted above, $\cot\alpha$ contributes an uncertainty range of ± 25 % which is comparable to or less than the typical statistical uncertainty in the determination of β.

To first order, the displacement-length scaling relation for shear-enhanced compaction bands is (6) neglecting the $\cot\alpha$ term. Noting from Table 2 that $\varepsilon_p = 0.066$ (Valley of Fire) or 0.0256 (Buckskin Gulch), the scaling relations are approximately $D_s = 1.25 \times 10^{-4} L^{1/2}$ and $D_s = 1.61 \times 10^{-4} L^{1/2}$ for shear-enhanced compaction bands at Valley of Fire and Buckskin Gulch respectively. The scaling relations may be interpreted as involving a process of band thickening during band growth at a constant value of plastic normal strain. This interpretation is consistent with the findings of Chemenda (2011) in his analyses of band localization and growth as a consequence of discontinuous bifurcation of material properties within a deforming host rock and qualitatively with the widening of shear zones in porous rocks as discussed by Aydin and Berryman (2010). The scaling of compactional shear bands is given simply by $D_s = AL^{1/2}$ (Schultz et al. 2008) where A may be related to host-rock stiffness and grain toughness.

5 Conclusions

Band propagation energies were calculated for several types of deformation bands from porous sandstone host rocks, including pure compaction bands, shear-enhanced compaction bands, and cataclastic compactional shear bands. Assuming small-scale yielding, the closing-mode propagation energies compare favorably with strain energy release rates obtained previously for shear-enhanced compaction bands. Shearing-mode propagation energies are comparable for shear-enhanced compaction bands and compactional shear bands despite differences in the magnitude of shear

displacement between them. Shear offsets along shear-enhanced compaction bands are consistent with those calculated trigonometrically from the band orientation and thickness, whereas those for compactional shear bands exceed the trigonometric values, implying an additional component of shearing offset in compactional shear bands associated with strain localization and a change in deformation mechanism in the bands. Displacement-length scaling of shear-enhanced compaction bands depends on band thickness and closing normal strain. The results suggest a correspondence between deformation mechanism (strain softening via cataclasis vs. stable shearing and grain rearrangement), evolving host-rock properties (grain size, shape, porosity), and far-field stress state with band type, consistent with findings in the literature.

Acknowledgments Thanks to Peter Eichhubl for discussions on compaction bands from the Valley of Fire site and to Alexandre Chemenda for discussions on compaction band localization and propagation. Reviews by two anonymous referees sharpened the final paper. This work was facilitated by a pleasant visiting professorship at the Université Montpellier and support by NASA's Planetary Geology and Geophysics Program, both to RAS while the first author was at the University of Nevada, Reno, which are gratefully acknowledged. Additional support was provided by consortium R&D project 429 207806/E20 (IMPACT; http://org.uib.no/cipr/Project/IMPACT) funded by the Research Council of Norway and Statoil. ConocoPhillips is thanked for granting permission to publish this work.

References

Atkinson BK, Meredith PG (1987) Experimental fracture mechanics data for rocks and minerals. In: Atkinson BK (ed) Fracture mechanics of rock. Academic Press, New York, pp 477–525

Aydin A, Berryman JG (2010) Analysis of the growth of strike-slip faults using effective medium theory. J Struct Geol 32:1629–1642

Aydin A, Borja RI, Eichhubl P (2006) Geological and mathematical framework for failure modes in granular rock. J Struct Geol 28:83–98

Aydin A, Schultz RA (1990) Effect of mechanical interaction on the development of strike-slip faults with echelon patterns. J Struct Geol 12:123–129

Ballas G, Soliva R, Sizun J-P, Benedicto A, Cavailhes T, Raynaud S (in press) The importance of the degree of cataclasis in shear bands for fluid flow in porous sandstone (Provence, France). Am Assoc Petrol Geol Bull. doi:10.1306/04051211097

Baud P, Vajdova V, Wong T-f (2006) Shear-enhanced compaction and strain localization: inelastic deformation and constitutive modeling of four porous sandstones. J Geophys Res 111:B12401. doi:10.1029/2005JB004101

Bésuelle P (2001) Compacting and dilating shear bands in porous rock: theoretical and experimental conditions. J Geophys Res 106:13435–13442

Borja RI, Aydin A (2004) Computational modeling of deformation bands in granular media. I. geological and mathematical framework. Comput Methods Appl Mech Eng 193:2667–2698

Chemenda AI (2009) The formation of tabular compaction-band arrays: theoretical and numerical analysis. J Mech Phys Solids 57:851–868

Chemenda AI (2011) Origin of compaction bands: anti-cracking or constitutive instability? Tectonophysics 499:156–164

Chemenda AI, Wibberley C, Saillet E (2012) Evolution of compactive shear localization bands: numerical models and geological data. Tectonophysics 526-529:56–66

Cowie PA, Scholz CH (1992) Physical explanation for the displacement-length relationship of faults using a post-yield fracture mechanics model. J Struct Geol 14:1133–1148

Cox SJD, Scholz CH (1988) Rupture initiation in shear fracture of rocks: an experimental study. J Geophys Res 93:3307–3320

Crouch SL, Starfield AM (1983) Boundary element methods in solid mechanics. Allen & Unwin, London

Das A, Nguyen GD, Einav I (2011) Compaction bands due to grain crushing in porous rocks: a theoretical approach based on breakage mechanics. J Geophys Res 116:B08203. doi:10.1029/2011JB008265

Davies TRH, McSaveney MJ, Boulton CJ (2012) Elastic strain energy release from fragmenting grains: effects on fault rupture. J Struct Geol 38:265–277

Du Y, Aydin A (1993) The maximum distortional strain energy density criterion for shear fracture propagation with applications to the growth paths of en échelon faults. Geophys Res Lett 20:1091–1094

Eichhubl P, Taylor WL, Pollard DD, Aydin A (2004) Paleo-fluid flow and deformation in the Aztec Sandstone at the Valley of Fire, Nevada: evidence for the coupling of hydrogeologic, diagenetic, and tectonic processes. Geol Soc Am Bull 116:1120–1136

Eichhubl P, Hooker JN, Laubach SE (2010) Pure and shear-enhanced compaction bands in Aztec Sandstone. J Struct Geol 32:1873–1886

Flodin EA, Aydin A (2004) Evolution of a strike-slip fault network, Valley of Fire State Park, southern Nevada. Geol Soc Am Bull 116:42–59

Fortin J, Stanchits S, Dresen G, Guéguen Y (2006) Acoustic emission and velocities associated with the formation of compaction bands in sandstone. J Geophys Res 111:B10203. doi:10.1029/2005JB003854

Fossen H, Schultz RA, Shipton ZK, Mair K (2007) Deformation bands in sandstone: a review. J Geol Soc Lond 164:755–769

Fossen H, Schultz RA, Torabi A (2011) Conditions and implications for compaction band formation in Navajo Sandstone, Utah. J Struct Geol 33:1477–1490

Gutierrez M (2011) Effects of constitutive parameters on strain localization in sands. Int J Num Anal Methods Geomech 35:161–178

Hasanpour R, Choupani N (2008) Mixed-mode study of rock fracture mechanics by using the modified Arcan specimen test. World Acad Sci Eng Tech 41:764–769

Hill RE (1989) Analysis of deformation bands in the Aztec Sandstone, Valley of Fire State Park, Nevada. MS thesis, Univ Nevada, Las Vegas

Hirth G, Tullis J (1989) The effects of pressure and porosity on the micromechanics of the brittle-ductile transition in quartzite. J Geophys Res 94:17825–17838

Holcomb D, Rudnicki JW, Issen KA, Sternlof K (2007) Compaction localization in the Earth and the laboratory: state of the research and research directions. Acta Geotech 2:1–15

Ikari MJ, Marone C, Saffer DM (2011) On the relation between fault strength and frictional stability. Geology 39:83–86

Jaeger JC, Cook NGW, Zimmerman RW (2007) Fundamentals of rock mechanics, 4th edn. Blackwell, London

Kanninen MF, Popelar CH (1985) Advanced fracture mechanics. Oxford University Press, Oxford

Kaproth BM, Cashman SM, Marone C (2010) Deformation band formation and strength evolution in unlithified sand: the role of grain breakage. J Geophys Res 115:B12103. doi:10.1029/2010JB007406

Karner SL, Chester FM, Kronenberg AK, Chester JS (2003) Subcritical compaction and yielding of granular quartz sand. Tectonophysics 377:357–381

Karner SL, Chester JS, Chester FM, Kronenberg AK, Hajash A Jr (2005) Laboratory deformation of granular quartz sand: implications for the burial of clastic rocks. Am Assoc Petrol Geol Bull 89:603–625

Kattenhorn SA, Pollard DD (1999) Is lithostatic loading important for the slip behavior and evolution of normal faults in the Earth's crust? J Geophys Res 104:28879–28898

Klimczak C, Soliva R, Schultz RA, Chéry J (2011) Growth of deformation bands in a multilayer sequence. J Geophys Res 116:B09209. doi:10.1029/2011JB008365

Lawn B (1993) Fracture of brittle solids, 2nd edn. Cambridge University Press, Cambridge

Li VC (1987) Mechanics of shear rupture applied to earthquake zones. In: Atkinson BK (ed) Fracture mechanics of rock. Academic Press, New York, pp 351–428

Mair K, Main I, Elphick S (2000) Sequential growth of deformation bands in the laboratory. J Struct Geol 22:25–42

Martel SJ, Pollard DD (1989) Mechanics of slip and fracture along small faults and simple strike-slip fault zones in granitic rock. J Geophys Res 94:9417–9428

Milliken KL, Reed RM, Laubach SE (2005) Quantifying compaction and cementation in deformation bands in porous sandstones. In: Sorkhabi R, Tsuji Y (eds) Faults, fluid flow, and petroleum traps. Am Assoc Petrol Geol Mem 85: 237–249

Mollema PN, Antonellini MA (1996) Compaction bands: a structural analog for anti-mode I cracks in aeolian sandstone. Tectonophysics 267:209–228

Okubo CH, Schultz RA (2006) Near-tip stress rotation and the development of deformation band stepover geometries in mode II. Geol Soc Am Bull 118:343–348

Olsson WA (1999) Theoretical and experimental investigation of compaction bands in porous rock. J Geophys Res 104:7219–7228

Olsson WA (2000) Origin of Lüders' bands in deformed rock. J Geophys Res 105:5931–5938

Olson EL, Cooke ML (2005) Application of three fault growth criteria to the Puente Hills thrust system, Los Angeles, California, USA. J Struct Geol 27:1765–1777

Palmer AC, Rice JR (1973) The growth of slip surfaces in the progressive failure of over-consolidated clay. Proc R Soc Lond A 332:527–548

Pollard DD, Aydin A (1988) Progress in understanding jointing over the past century. Geol Soc Am Bull 100:1181–1204

Pollard DD, Segall P (1987) Theoretical displacements and stresses near fractures in rock: with applications to faults, joints, dikes, and solution surfaces. In: Atkinson BK (ed) Fracture mechanics of rock. Academic Press, New York, pp. 277–349

Rice JR (1968) A path independent integral and the approximate analysis of strain concentration by notches and cracks. J Appl Mech 35:379–386

Rice JR, Simons DA (1976) The stabilization of spreading shear faults by coupled deformation-diffusion effects in fluid-infiltrated porous materials. J Geophys Res 81:5322–5334

Rudnicki JW (1980) Fracture mechanics applied to the Earth's crust. Ann Rev Earth Planet Sci 8:489–525

Rudnicki JW (2007) Models for compaction band propagation. In: David C, Le Ravalec-Dupin M (eds) Rock physics and geomechanics in the study of reservoirs and repositories. Geol Soc London Spec Publ 284:107–125

Rudnicki JW, Sternlof KR (2005) Energy release model of compaction band propagation. Geophys Res Lett 32:L16303. doi:10.1029/2005GL023602

Saillet E (2009) La localisation de la déformation dans les grès poreux: caractérisation d'un analogue de réservoir gréseux et faillé dans le Bassin du Sud-Est, Provence, France. Unpublished Docteur en Sciences thesis, Université de Nice-Sophia Antipolis

Saillet E, Wibberley CAJ (2010) Evolution of cataclastic faulting in high-porosity sandstone, Bassin du Sud-Est, Provence, France. J Struct Geol 32:1590–1608

Schultz RA (2009) Scaling and paleodepth of compaction bands, Nevada and Utah. J Geophys Res 114:B03407. doi:10.1029/2008JB005876

Schultz RA (2011) Relationship of compaction bands in Utah to Laramide fault-related folding. Earth Planet Sci Lett 304:29–35

Schultz RA, Balasko CM (2003) Growth of deformation bands into echelon and ladder geometries. Geophys Res Lett 30:3033. doi:10.1029/2003GL018449

Schultz RA, Soliva R, Fossen H, Okubo CH, Reeves DM (2008) Dependence of displacement-length scaling relations for fractures and deformation bands on the volumetric changes across them. J Struct Geol 30:1405–1411

Schultz RA, Okubo CH, Fossen H (2010) Porosity and grain size controls on compaction band formation in Jurassic Navajo Sandstone. Geophys Res Lett 37:L22306. doi:10.1029/2010GL044909

Smith PR, Jardine RJ, Hight DW (1992) The yielding of Bothkenar clay. Géotechnique 42:257–274

Soliva R, Schultz RA, Ballas G, Taboada A, Saillet E, Wibberley C, Benedicto A (2011) The relationship between deformation band properties, tectonic regime and burial in porous sandstone. Geophys Res Abstr 13:EGU/2011–6377

Soliva R, Schultz RA, Ballas G, Taboada A, Wibberley C, Saillet E, Benedicto A (in press) A model of strain localization in porous sandstone as a function of tectonic setting, burial and material properties; new insight from Provence (southern France). J Struct Geol

Solum JG, Brandenburg JP, Kostenko OV, Wilkins SJ, Schultz RA (2010) Characterization of deformation bands associated with normal and reverse stress states in the Navajo Sandstone, Utah. Am Assoc Petrol Geol Bull 94:1453–1475

Stanchits S, Fortin J, Gueguen Y, Dresen G (2009) Initiation and propagation of compaction bands in dry and wet Bentheim Sandstone. Pure Appl Geophys 166:843–868

Sternlof KR, Rudnicki JW, Pollard DD (2005) Anticrack inclusion model for compaction bands in sandstone. J Geophys Res 110:B11403. doi:10.1029/2005JB003764

Sutton MA, Deng X, Ma F, Newman JC Jr, James M (2000) Development and application of a crack tip opening displacement-based mixed mode fracture criterion. Int J Solids Struct 37:3591–3618

Sylte JE, Thomas LK, Rhett DW, Bruning DD, Nagel NB (1999) Water induced compaction in the Ekofisk Field. SPE paper 56426

Tembe S, Vajdova V, Wong T-f, Zhu W (2006) Initiation and propagation of strain localization in circumferentially notched samples of two porous sandstones. J Geophys Res 111:B02409. doi:10.1029/2005JB003611

Tembe S, Baud P, Wong T-f (2008) Stress conditions for the propagation of discrete compaction bands in porous sandstone. J Geophys Res 113:B09409. doi:10.1029/2007JB005439

Togo T, Simamoto T (2012) Energy partition for grain crushing in quartz gouge during subseismic to seismic fault motion: an experimental study. J Struct Geol 38:139–155

Torabi A, Alikarami R (2012) Heterogeneity within deformation bands in sandstone reservoirs. Amer Rock Mech Assoc paper ARMA 12–347

Vajdova V, Wong T-f (2003) Incremental propagation of discrete compaction bands: acoustic emission and microstructural observations on circumferentially notched samples of Bentheim Sandstone. Geophys Res Lett 30:1775. doi:10.1029/2003GL017750

Wibberley CAJ, Petit J-P, Rives T (2007) The mechanics of fault distribution and localization in high-porosity sands, Provence, France. In: Lewis H, Couples GD (eds) The relationship between damage and localization Geol Soc London Spec Publ 289:19–46

Wong T-f (1982) Shear fracture energy of Westerly granite from post failure energy. J Geophys Res 87:990–1000

Yoda M (1980) The J-integral fracture toughness for mode II. Int J Frac 16:R175–R178